ISSN 1063-7710, Acoustical Physics, 2019, Vol. 65, No. 5, pp. 471–477. © Pleiades Publishing, Ltd., 2019.

PHYSICAL ACOUSTICS

Ambient Acoustic Energy Harvesting using Two Connected Resonators with Piezoelement for Wireless Distributed Sensor Network

Iftikhar Ahmad[a], Adnan Hassan[a, *], Muneeb Ullah Anjum[b], Sohail Malik[a], and Tashfeen Ali[c]

[a] *Faculty of Mechanical Engineering, Ghulam Ishaq Khan Institute of Engineering Sciences and Technology, Topi, Pakistan*

[b] *Electrical Engineering Department, COMSATS Institute of Information Technology, Islamabad, 45550 Pakistan*

[c] *Network Support Engineer, Nayatel Private Limited, Islamabad, Pakistan*

**e-mail: adhassan@ku.edu.tr*

Received October 7, 2018; revised January 9, 2019; accepted May 7, 2019

Abstract—In this article, an acoustic energy harvester (AEH) is conceptualized, designed, fabricated and tested. The developed AEH (DAEH) consists of two Helmholtz cavities (HCs) and a commercially available piezoelement. The HCs were fabricated from Teflon material using conventional machining operations. An indigenous test bench for in-lab characterization of DAEH has also been developed. Various experiments were performed to experimentally record the frequency response function, loading and power characteristics. Additionally, the in-lab and open-air characterization of the DAEH is also reported. Furthermore, the proposed prototype of DAEH is compared on the basis of various benchmarks with the prototypes available in the literature. The experimental results indicate a maximum power density of 32.7 $\mu W/cm^3$ at 130 dB.

Keywords: acoustic, energy harvesting, piezoelectric, wireless sensor node

DOI: 10.1134/S1063771019050014

INTRODUCTION

Wireless distributed sensor network (WDSN) is widely used in weather forecasting [1], traffic control [2], condition monitoring of industrial machines [3] and structural health monitoring of bridges [4]. One of the main component of the WDSN is wireless sensor node (WSN) [5]. The architecture of WSN is shown in Figure 1. WSN consists of a sensor unit, signal conditioning unit, wireless transmitter unit, power management unit, microcontroller unit and a battery for power up. In WDSN, the main power consumption unit is WSN as it sends and receives data continuously [6]. WSNs use battery as sole power source which has a lot of problems like finite shelf life, deep discharge, charging point requirements, etc. [7]. However, the periodic replacement of batteries in WDSN becomes very difficult because of its distribution over the vast area.

The on-going research either focuses to increase the battery life or to replace the batteries with some alternatives [8, 9]. Moreover, various types of ambient energy sources are available in the vicinity of WSNs which can be harvested for the power requirement of WSNs. Researchers have developed vibration [10], thermoelectric [11], wind [12] and solar [13] energy harvesters to power up WSNs. Acoustic energy is also abundantly available in the surrounding of WSNs [14], however, a limited research has been done on acoustic energy harvesters (AEHs). Sound pressure level (*SPL*) of various acoustic energy sources reported in the literature has been summarized in Table 1.

In [21], an electromagnetic type AEH was developed for handy electronics devices. The harvester has been developed using neodymium magnet and a nickel planar spring and coil. With an overall volume of 9 mm^3, the developed prototype was able to produce a maximum open circuit voltage (OCV) of 0.24 mV. A piezoelectric type AEH has been discussed in [22]. The developed device was able to harvest maximum voltage of 5.8 mV and power of 0.00048 μW at a matching impedance of 400 kΩ. Furthermore, experimental and numerical analysis of low frequency AEH was studied in [23]. The developed prototype was able to generate an output voltage of 5089 mV at an incident *SPL* of 100 dB. Most of the AEHs reported in literature [24–27] have very low output power due to optimal design and shape of the harvester.

In summary, there are three major motivations for the work presented in this article. First, the existing WDSNs majorly rely on limited power supply and the battery has a finite lifespan. Second, most of the work considering acoustic energy harvesting focuses on the voltage but does not concern the power density. Third, the two HCs can be used to obtain maximum oscillations.

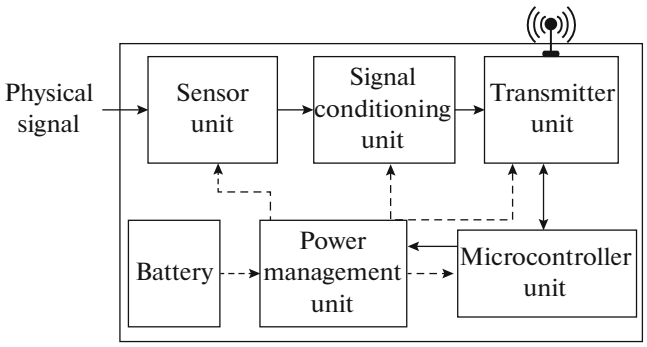

Fig. 1. Architecture of wireless sensor node (WSN).

Statement of contribution: In this paper, we study the acoustic energy harvesting solutions for the WDSNs where power to the nodes can be scavenged from the acoustic sources present at their surroundings. A prototype of DAEH having size almost equal to the normal headphone mic is conceptualized, designed, fabricated and tested both in laboratory and open air environment. Additionally, the proposed prototype has novelty in terms of its ability to generate maximum power due to the optimized shape of having two Helmholtz cavities (HCs) in a small volume.

PHYSICAL PRINCIPLES AND FABRICATION OF THE DEVICE

The cross-sectional view of the DAEH is shown in Fig. 1a. The DAEH comprises of the front cavity, bimorph circular piezoelement and a back cavity. The electrical connections have been taken from piezoelement through the back cavity. CAD model of the device is shown in Fig. 2b. The main function of the front cavity is to boost the amplitude of acoustic waves. When sound pressure is applied through the hole of front cavity, the air moves toward the piezoelement from its equilibrium position and the pressure inside the front cavity increases that deforms the piezoelement. When the piezoelement reaches its extreme position, pressure develops in the back cavity and it pushes the piezoelement in upward direction and because of this oscillation, a voltage is induced across the electrodes of piezoelement. Moreover, a maximum voltage is generated when the resonance of the piezoelement is achieved [28].

Table 1. Sound pressure level of different acoustic energy source

Acoustic energy source	Sound pressure level, dB	Ref.
Aircraft	115	[15]
Train moving with 200 km/hr	140	[16]
MRI scanner (3T)	130.7	[17]
Textile manufacturing industry	110	[18]
Pneumatic hammer	131	[19]
Glass industry	113	[20]

The HC is modeled as a spring-mass-damper system. The air vibrating in the hole of the HC has kinetic energy. The hole of the HC is assumed as a circular pipe which offers resistance to the moving air in it. The air present in the HC is modeled as a spring because of its compressibility (storing the potential energy). With the help of the physics related to the piezoelement, this energy is transformed into electrical energy. Several researchers has developed the electrical circuit equivalent of the piezoelement with similar loading characteristics. This article presents a coupled transfer function of the load current with respect to the oscillation amplitude with the help of the equivalent models presented in [29].

The free-body diagram of the system is shown in Fig. 2c. The mass M of the vibrating element is coupled with the spring K and damper c as shown. S_0P_{inc} is the force exerted on the piezoelement which is the product of the incoming pressure P_{inc} and the surface area S_0. The reflected pressure P_R causes a reactional force as shown in the figure and the transmitted force on the system is the difference between these two forces. The overall mechanical model of the system is given by [29]:

$$M\ddot{u} + c\dot{u} + K_E u = S_0 P_{\text{tot}} - \alpha V, \tag{1}$$

where $u, \dot{u}$ and $\ddot{u}$ are the displacement, velocity and the acceleration of the vibrating element, K_E is the effective stiffness of the system, α is the force factor, P_{tot} is the sum of P_{inc} and P_R. Performing the Laplace transformation on Eq. (1) yields the following:

$$s^2 MU(s) + scU(s) + K_E U(s) = S_0 P_{\text{tot}} - \alpha V(s). \tag{2}$$

The electrical equivalent is shown in Fig. 2d. In order to model the electrical system, the vibrating structure is connected to a load resistor R_L through a bridge rectifier via a smoothing capacitor C_s. The electrical model [29] is given by Eq. (3) and the Laplace transformation is shown in eq.(4):

$$i(t) = \alpha\dot{u} - C_0\dot{V}, \tag{3}$$

$$I(s) = s\alpha U(s) - sC_0 V(s), \tag{4}$$

$$V(s) = \frac{s\alpha U(s) - I(s)}{sC_0}. \tag{5}$$

Here an assumption is made that the load current increases linearly with the increase of the applied acoustical force with a factor β with non-hysteresis characteristics. This would equate S_0P_{tot} with βI. Therefore, Eq. (2) becomes:

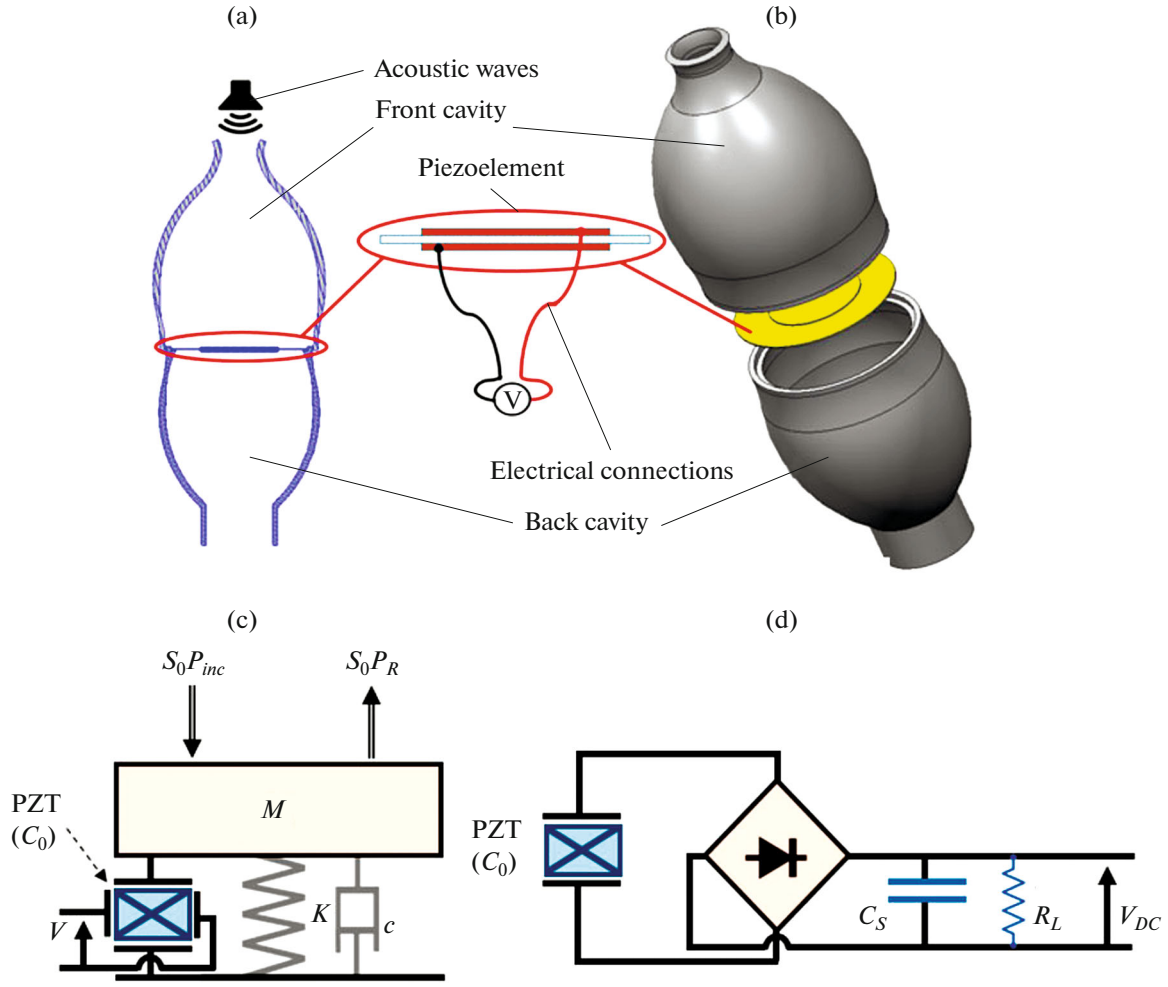

Fig. 2. Acoustic energy harvester (a)—cross sectional view, (b)—CAD model, (c)—free-body diagram, (d)—electrical circuit equivalent.

$$s^2MU(s) + scU(s) + K_EU(s) = \beta I - \alpha V(s). \quad (6)$$

Relating Eq. (2) and Eq. (6) results in the following Eq. (7)–Eq. (9):

$$s^2MU(s) + sCU(s) + K_EU(s) = \beta I - \alpha\left[\frac{s\alpha U(s) - I(s)}{sC_0}\right], \quad (7)$$

$$\left[s^2M + sC + K_E + \frac{\alpha^2}{C_0}\right]U(s) = \left[\beta + \frac{\alpha}{sC_0}\right]I(s), \quad (8)$$

$$\frac{I(s)}{U(s)} = \frac{s^3MC_0 + s^2CC_0 + s\left(K_EC_0 + \alpha^2\right)}{s\beta C_0 + \alpha}, \quad (9)$$

where Eq. (9) represents the transfer function of the load current to the displacement of the vibrating element. The undamped resonant frequency of the HC [30] is given by:

$$F_{\text{Undamped}} = \frac{C}{2\pi}\sqrt{\frac{3A_h}{4V_cL_h}}, \quad (10)$$

where C is the speed of sound, A_h is the cross sectional area of the hole, V_c is the volume of the HC and L_h is the length of the hole. Moreover, [31] was studied to obtain the geometric parameters of the HC.

The device is composed of two cavities (front and back), both of which are fabricated from commercially available Teflon rod. A conventional machining is performed on a Teflon rod having a dimeter of 14 mm. The bottom cavity having length of 7 mm and maximum diameter 13 mm is fabricated in such a way that a piezoelement can be placed on the top of the cavity. Commercially available piezoelement is used for electromechanical transduction. The piezoelement comprises of 0.1 mm thick brass layer and two Lead Zirconate Titanate (PZT) layers attached on each side of brass plate. The fabrication and assembling process of the DAEH is illustrated in Fig. 3. The fabrication of the front cavity through turning machine is shown in

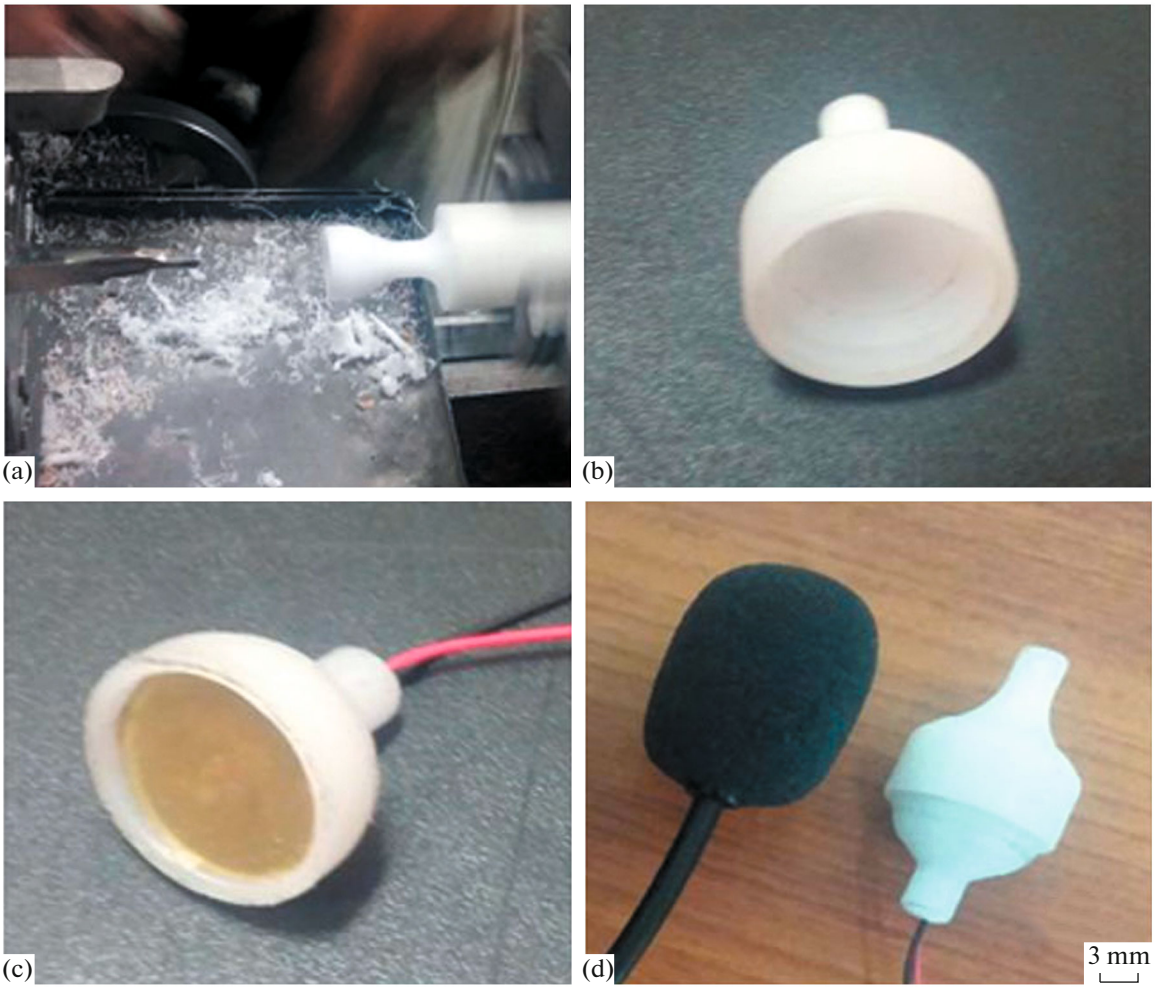

Fig. 3. Fabrication and assembling flow of the DAEH (a)—fabrication of front cavity through turning machine, (b)—fabricated front cavity, (c)—piezo element in back cavity, (d)—assembled prototype in comparison with headphone mic.

Fig. 3a. Fabricated cavities and piezoelement placed in back cavity are depicted in Fig. 3b,c respectively. Side view of the assembled device in comparison with the headphone mic is shown in Fig. 3d. Dimensions and parameters of the DAEH are listed in Table 2.

Table 2. Dimensions and parameter of the DAEH

Descriptions	Value	Unit
Front cavity length	12	mm
Front cavity dimeter	12	mm
Front cavity hole dimeter	2	mm
Front cavity hole length	4	mm
Back cavity length	7	mm
Back cavity diameter	13	mm
Total thickness of piezo element	360	μm
Thickness of PZT	260	μm
Thickness of brass	100	μm
Dimeter of PZT ceramics	12	mm
Dimeter of brass	18	mm

EXPERIMENT

The experimental setup developed in this research for the characterization of DAEH is shown in Fig. 4. The setup comprises of a speaker (sound source), ROHDE and SCHWARZ®-HMO-1202 function generator (to regulate the frequency and amplitude of acoustic wave), power amplifier (for amplification of acoustic wave), plane wave tube (ensures smooth sinusoidal acoustic wave [32]), HHSL-1 OMEGA™ sound meter (to measure the *SPL* of acoustic wave), National Instruments™ MyRIO-1900 Data acquisition card (to acquire the output voltage of the DAEH), variable resistor (for load voltage analysis) and a computer with LabVIEW (to record and save data from DAQ card). The sound wave passes through the plane wave tube and strikes the DAEH, *SPL* is measured

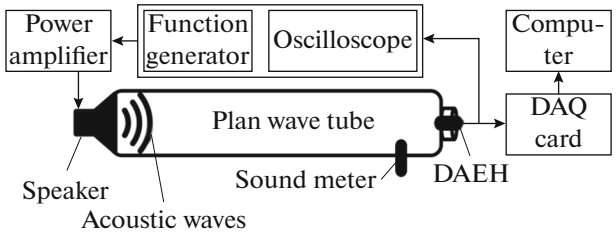

Fig. 4. Experimental setup block diagram.

using sound meter placed near the DAEH. The output voltage is analyzed in LabVIEW software.

The DAEH has been tested under different *SPL* of sinusoidal acoustic wave. Output OCV, output load voltage and output load power analysis have been performed during the characterization. The OCV versus frequency at various *SPL* is depicted in Fig. 5. The DAEH was characterized at a frequency sweep from 600 to 1800 Hz under *SPL* of 110, 120 and 130 dB. It can be seen from Fig. 5 that when the device is subjected to *SPL* of 130 dB, it produces a maximum OCV of 558 mV at a frequency of 1354 Hz. However, at the same frequency the device able to generate an OCV of 228 and 95 mV when subjected to *SPL* of 120 and 110 dB respectively.

Figure 6 shows the output load voltage versus load resistance for DAEH at various *SPL*. A linear variable resister is used to change the external load. By varying the load resistance, the load voltage increase at the expense of decease in the output current through the resistor. At *SPL* of 130 dB, the prototype is able to generate a maximum load voltage of 470 mV at matching impedance of 24000 Ω. Moreover, the output power of DAEH under different *SPL* was also calculated using this equation,

$$P = \frac{V_{rms}^2}{R_L}, \tag{11}$$

and is depicted in Fig. 7. It was observed that maximum output power of 40 μW was achieved for load resistance of 1200 Ω at 130 dB of *SPL*.

The DAEH has also been characterized in an open environment at a constant frequency equal to the third peak (13.5 kHz) in Fig. 5, using the setup shown in Fig. 8a. The DAEH and sound meter are placed firmly near to each other in a stand. In order to validate the reliance of AEH on distance with respect to the acoustic source, the device is moved away from the acoustic source. The OCV and *SPL* as a function of distance are shown in Fig. 8b. At *SPL* of 120 dB, a maximum OCV of 200 mV is generated when the device is sited at a minimum distance from the acoustic source. Whereas, at *SPL* of 66 dB, AEH generates 33 mV OCV at a maximum distance of 200 mm. The voltage generation decrease considerably as the harvester is moved away from the source.

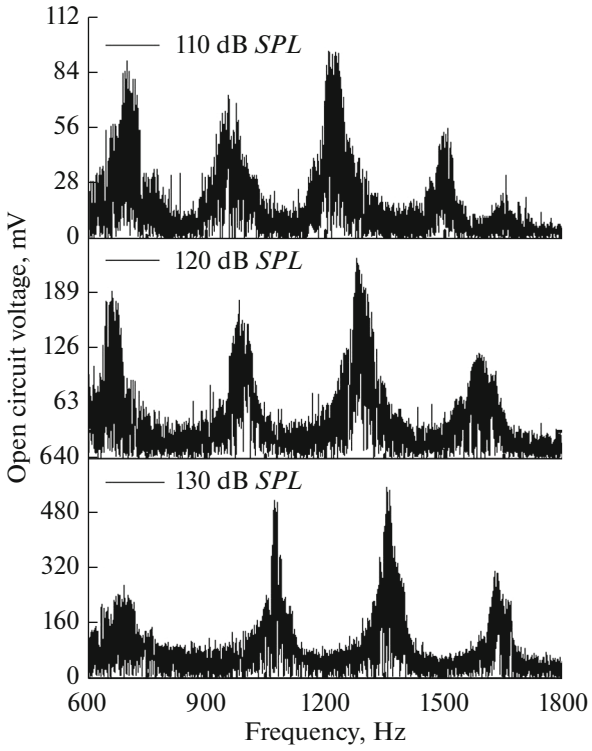

Fig. 5. Open circuit voltage as a function of frequency at different sound pressure level.

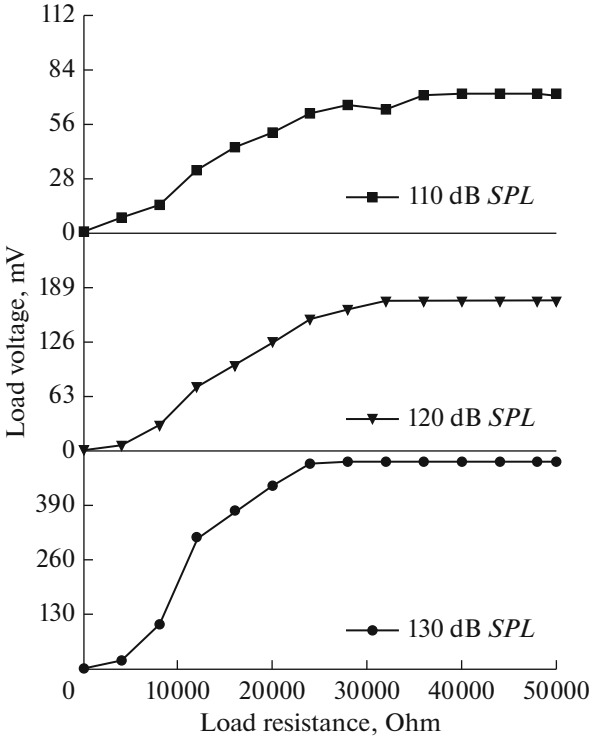

Fig. 6. Load voltage as a function of load resistance at different sound pressure level.

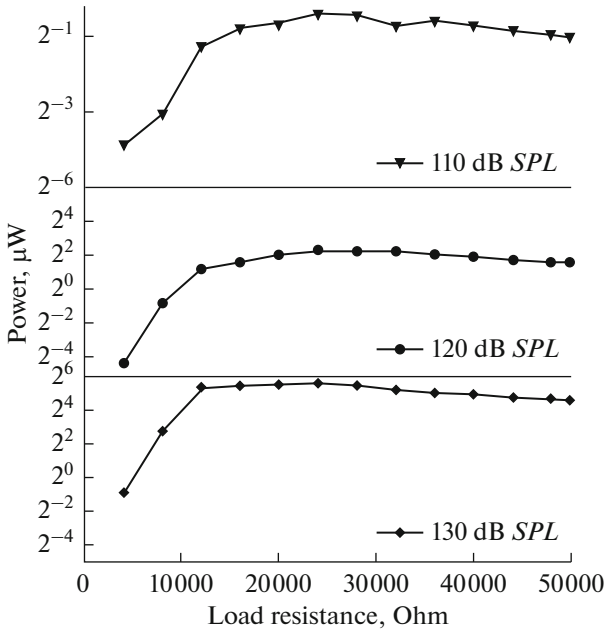

Fig. 7. Power as a function of load resistance at different sound pressure level.

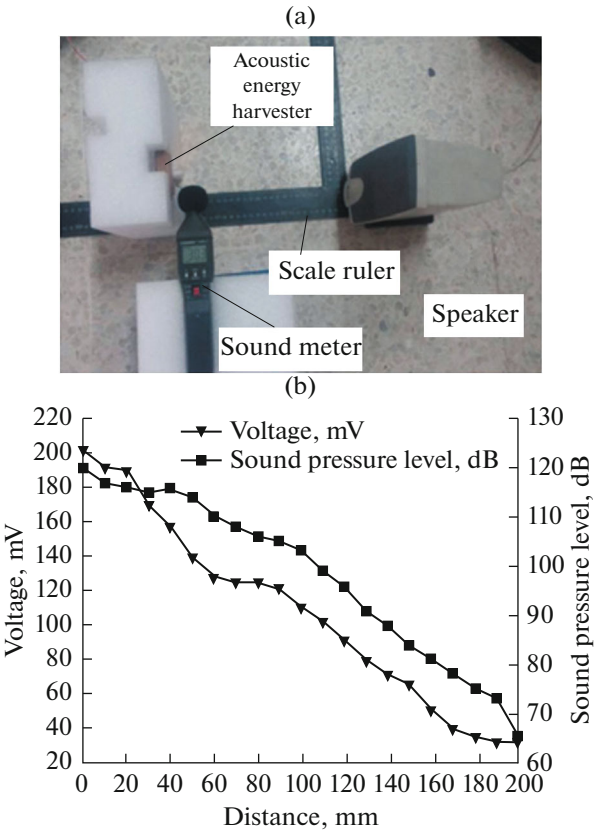

Fig. 8. Open environment experiment (a)—experimental setup, (b)—OCV and sound pressure level as a function of distance.

The excitation frequency plays a vital role in generation of the electrical energy. With the help of the transfer function presented in Eq. (9), the generalized bode plot is shown in Fig. 9. The result of piezoelement excitation at the resonance exhibits the phase reversal as well as the highest amplitude of the electrical current across load is generated.

COMPARISON WITH PREVIOUS WORK

The developed AEH has been compared with the reported work done in the literature. The prototype fabricated in this research have been matched by various benchmarks such as dimension of prototype, *SPL*, frequency, resistance, output voltage, power and power density. Various parameters of the AEHs reported and developed in this work have been summarized in Table 3. It has been observed that the output voltage of the DAEH is higher than the harvesters developed in [21, 22, 24–27], however, the AEH developed in [23] has higher output voltage then the

Table 3. Parameters of various reported AEHs

Dimensions, cm^3	*SPL*, dB	Frequency, kHz	Internal resistance, kΩ	Output voltage, mV	Power, μW	Power density, $\mu W/cm^3$	Ref.
0.009	—	0.4		0.24	—	—	[21]
—	—	—	400	5.8	0.00048	—	[22]
5.60	110	199	4.6	15600	12600	15.15	[23]
—	—	4.2	3.9	18	0.04	—	[24]
11.52	—	4.3	30	30	0.036	0.0031	[25]
0.048*	100	16.7	0.075	—	0.00014	0.0029	[26]
3.8**	149	13.6	0.980	—	0.01	0.34	[27]
1.22	130	13.5	12	558	40	32.7	[DAEH]

* Estimated size;
** Length in cm;
*** Unit is $\mu W/cm^2$.

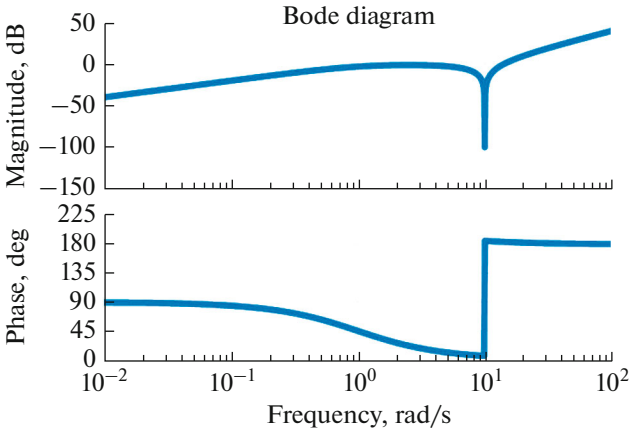

Fig. 9. Generalized bode-plot of the coupled electromechanical system.

DAEH proposed in this research which is due to the larger size of the device developed in [23], and therefore the power density of the [23] (15.15 μW/cm^3) is less than the proposed prototype (32.7 μW/cm^3). Furthermore, it is observed that the prototype developed in this work has highest power density among all the reported prototypes except [21, 22, 24]. In [21], the authors have not analyzed the load voltage, while, in [22] and [24], the device size is not reported, however the output power (0.00048 μW [22], 0.04 μW [24]) is less than the propped DAEH (40 μW).

CONCLUSION

The development and in-lab characterization of the developed acoustic energy harvester (DAEH) has been illustrated in this paper. The prototype having overall size almost equal to a normal headphone mic was successfully developed and tested. The DAEH was subjected to a frequency sweep of 600 to 1800 Hz at *SPL* of 110, 120 and 130 dB. The device was able to generate a maximum power density of 32.7 μW/cm^3 when subjected to *SPL* of 130 dB. The DAEH having a novel structure of two Helmholtz cavities has also been compared with the reported AEHs and it was observed that the proposed device is able to have maximum power density than all of the reported AEHs.

REFERENCES

1. T. Arampatzis, J. Lygeros, and S. Manesis, in *Proc. 2005 IEEE Int. Symposium on Intelligent Control and 13th Mediterranean Conference on Control and Automation* (Limassol, 2005), pp. 719–724.
2. C.-Y. Chong and S. P. Kumar, Proc. IEEE **91**, 1247 (2003).
3. F. Salvadori, M. de Campos, P. S. Sausen, R.F. de Camargo, C. Gehrke, C. Rech, et al., IEEE Trans. Instrum. Meas. **58**, 3104 (2009).
4. T. Harms, S. Sedigh, and F. Bastianini, IEEE Instrum. Meas. Mag. **13**, 14 (2010).
5. F. Khan and Izhar, J. Renewable Sustainable Energy **8**, 054701 (2016).
6. G. Lu, B. Krishnamachari, and C. S. Raghavendra, in Proc. 18th IEEE Int. Parallel and Distributed Processing Symposium (Santa Fe, NM, 2004), p. 224.
7. F. U. Khan and I. Ahmad, Shock Vib., **2016**, Article ID 1340402 (2016).
8. F. K. Shaikh and S. Zeadally, J. Renewable Sustainable Energy Rev. **55**, 1041 (2016).
9. F. U. Khan, Sens. Rev. **38** (3), 298 (2018).
10. F. U. Khan and I. Ahmad., in *Proc. 10th Int. Conference on Emerging Technologies 2014* (*ICET 2014*) (Islamabad, 2014), p. 125.
11. D. Samson, M. Kluge, T. Becker, and U. Schmid, Sens. Actuators, A **172**, 240 (2011).
12. F. U. Khan and M. Iqbal, in *Proc. Int. Conference on Intelligent Systems Engineering (ICISE)* (Islamabad, 2016), p. 380.
13. P. Srinivas and K. V. Lakshmi, Sol. Energy **5** (6), 2017 (2017).
14. F. U. Khan, J. Micromech. Microeng. **25**, 023001 (2015).
15. Y. Yokoyama and K. Hashimoto, JR East Tech. Rev. **16**, 63 (2010).
16. X. Hu, T. Aoki, and N. Tokura, Open J. Fluid Dyn. **2**, 285 (2012).
17. Y. Hattori, H. Fukatsu, and T. Ishigaki, Nagoya J. Med. Sci. **69**, 23 (2007).
18. R. Bedi, Ind. Health **44**, 112 (2006).
19. P. Nassiri, R. Gol-Mohammadi, and P. Kamali, J. Phys. IV **2**, C1-531 (1992).
20. J. Pekkarinen, Am. Ind. Hyg. Assoc. J. **48**, 861 (1987).
21. T. Lai, C. Huang, and C. Tsou, in *Proc. 2008 Symposium on Design, Test, Integration and Packaging of MEMS/MOEMS* (Nice, 2008), p. 28.
22. S. Susilo, A. Putra, and S. L. Kok, Appl. Mech. Mater. **695**, 757 (2014).
23. B. Li, H. J. You, and Y.-J. Kim, Smart Mater. Struct. **22**, 055013 (2013).
24. L.-Y. Wu, L.-W. Chen, and C.-M. Liu, Appl. Phys. Lett. **95**, 013506 (2009).
25. W.-C. Wang, L.-Y. Wu, L.-W. Chen, and C.-M. Liu, Smart Mater. Struct. **19**, 045016 (2010).
26. S. Kimura, S. Tomioka, S. Iizumi, K. Tsujimoto, T. Sugou, and Y. Nishioka, Jpn. J. Appl. Phys. **50**, 06GM14 (2011).
27. S. B. Horowitz, M. Sheplak, L. N. Cattafesta III, and T. Nishida, J. Micromech. Microeng.s **16**, S174 (2006).
28. D. Wu, Y. Dai, H. Chen, Y. Zhou, L. Fu and X. Wang, Acoust. Phys. **63** (5), 617 (2017).
29. M. Lallart, D. Guyomar, C. Richard and L. Petit, J. Acoust. Soc. Am. **128** (5), 2739 (2010).
30. A. Nolle, J. Acoust. Soc. Am. **25**, 32 (1953).
31. A. I. Komkin, M. A. Mironov, and A. I. Bykov, Acoust. Phys. **63** (4), 385 (2017).
32. L. A. Tkachenko and S. A. Fadeev, Acoust. Phys. **63** (1), 7 (2017).